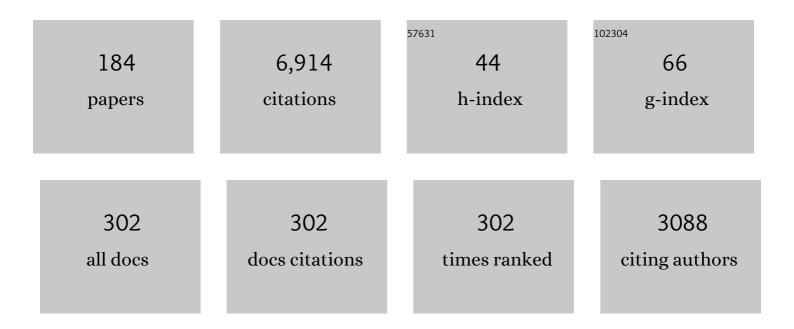
## Martin Riese

List of Publications by Year in descending order

Source: https://exaly.com/author-pdf/669118/publications.pdf Version: 2024-02-01



#	Article	IF	CITATIONS
1	Impact of uncertainties in atmospheric mixing on simulated UTLS composition and related radiative effects. Journal of Geophysical Research, 2012, 117, .	3.3	260
2	Space-based measurements of stratospheric mountain waves by CRISTA 1. Sensitivity, analysis method, and a case study. Journal of Geophysical Research, 2002, 107, CRI 6-1-CRI 6-23.	3.3	227
3	Implications for atmospheric dynamics derived from global observations of gravity wave momentum flux in stratosphere and mesosphere. Journal of Geophysical Research, 2011, 116, .	3.3	203
4	Cryogenic Infrared Spectrometers and Telescopes for the Atmosphere (CRISTA) experiment and middle atmosphere variability. Journal of Geophysical Research, 1999, 104, 16311-16325.	3.3	177
5	Cryogenic Infrared Spectrometers and Telescopes for the Atmosphere (CRISTA) data processing and atmospheric temperature and trace gas retrieval. Journal of Geophysical Research, 1999, 104, 16349-16367.	3.3	130
6	Global ray tracing simulations of the SABER gravity wave climatology. Journal of Geophysical Research, 2009, 114, .	3.3	120
7	Implications of Satellite OH Observations for Middle Atmospheric H2O and Ozone. Science, 1997, 277, 1967-1970.	6.0	114
8	Tropospheric ozone trend over Beijing from 2002–2010: ozonesonde measurements and modeling analysis. Atmospheric Chemistry and Physics, 2012, 12, 8389-8399.	1.9	111
9	Contribution of mixing to upward transport across the tropical tropopause layer (TTL). Atmospheric Chemistry and Physics, 2007, 7, 3285-3308.	1.9	109
10	Interaction of gravity waves with the QBO: A satellite perspective. Journal of Geophysical Research D: Atmospheres, 2014, 119, 2329-2355.	1.2	109
11	Tropical troposphere to stratosphere transport of carbon monoxide and long-lived trace species in the Chemical Lagrangian Model of the Stratosphere (CLaMS). Geoscientific Model Development, 2014, 7, 2895-2916.	1.3	104
12	Horizontal water vapor transport in the lower stratosphere from subtropics to high latitudes during boreal summer. Journal of Geophysical Research D: Atmospheres, 2013, 118, 8111-8127.	1.2	100
13	Fast transport from Southeast Asia boundary layer sources to northern Europe: rapid uplift in typhoons and eastward eddy shedding of the Asian monsoon anticyclone. Atmospheric Chemistry and Physics, 2014, 14, 12745-12762.	1.9	97
14	Ammonium nitrate particles formed in upper troposphere from ground ammonia sources during Asian monsoons. Nature Geoscience, 2019, 12, 608-612.	5.4	95
15	GRACILE: a comprehensive climatology of atmospheric gravity wave parameters based on satellite limb soundings. Earth System Science Data, 2018, 10, 857-892.	3.7	91
16	Towards a 3-D tomographic retrieval for the air-borne limb-imager GLORIA. Atmospheric Measurement Techniques, 2010, 3, 1647-1665.	1.2	90
17	Reconciliation of essential process parameters for an enhanced predictability of Arctic stratospheric ozone loss and its climate interactions (RECONCILE): activities and results. Atmospheric Chemistry and Physics, 2013, 13, 9233-9268.	1.9	88
18	Gimballed Limb Observer for Radiance Imaging of the Atmosphere (GLORIA) scientific objectives. Atmospheric Measurement Techniques, 2014, 7, 1915-1928.	1.2	85

#	Article	IF	CITATIONS
19	The CRISTA-2 mission. Journal of Geophysical Research, 2002, 107, CRI 1-1-CRI 1-12.	3.3	84
20	Instrument concept of the imaging Fourier transform spectrometer GLORIA. Atmospheric Measurement Techniques, 2014, 7, 3565-3577.	1.2	82
21	Horizontal transport affecting trace gas seasonality in the Tropical Tropopause Layer (TTL). Journal of Geophysical Research, 2012, 117, .	3.3	80
22	A microphysics guide to cirrus – Part 2: Climatologies of clouds and humidity from observations. Atmospheric Chemistry and Physics, 2020, 20, 12569-12608.	1.9	80
23	Characteristics of gravity waves resolved by ECMWF. Atmospheric Chemistry and Physics, 2014, 14, 10483-10508.	1.9	78
24	A potential vorticity-based determination of the transport barrier in the Asian summer monsoon anticyclone. Atmospheric Chemistry and Physics, 2015, 15, 13145-13159.	1.9	78
25	Tropopause to mesopause gravity waves in August: Measurement and modeling. Journal of Atmospheric and Solar-Terrestrial Physics, 2006, 68, 1730-1751.	0.6	77
26	Envisat MIPAS measurements of CFC-11: retrieval, validation, and climatology. Atmospheric Chemistry and Physics, 2008, 8, 3671-3688.	1.9	77
27	Role of gravity waves in the forcing of quasi twoâ€day waves in the mesosphere: An observational study. Journal of Geophysical Research D: Atmospheres, 2013, 118, 3467-3485.	1.2	76
28	Impact of different Asian source regions on the composition of the Asian monsoon anticyclone and of the extratropical lowermost stratosphere. Atmospheric Chemistry and Physics, 2015, 15, 13699-13716.	1.9	75
29	Insight from ozone and water vapour on transport in the tropical tropopause layer (TTL). Atmospheric Chemistry and Physics, 2011, 11, 407-419.	1.9	71
30	Quantifying the effects of mixing and residual circulation on trends of stratospheric mean age of air. Geophysical Research Letters, 2015, 42, 2047-2054.	1.5	69
31	GLObal limb Radiance Imager for the Atmosphere (GLORIA): Scientific objectives. Advances in Space Research, 2005, 36, 989-995.	1.2	68
32	New perspectives on gravity wave remote sensing by spaceborne infrared limb imaging. Atmospheric Measurement Techniques, 2009, 2, 299-311.	1.2	63
33	A 3-D tomographic retrieval approach with advection compensation for the air-borne limb-imager GLORIA. Atmospheric Measurement Techniques, 2011, 4, 2509-2529.	1.2	61
34	Quantifying pollution transport from the Asian monsoon anticyclone into the lower stratosphere. Atmospheric Chemistry and Physics, 2017, 17, 7055-7066.	1.9	61
35	Long-term changes of methane and hydrogen in the stratosphere in the period 1978–2003 and their impact on the abundance of stratospheric water vapor. Journal of Geophysical Research, 2006, 111, .	3.3	59
36	Satellite observations of middle atmosphere gravity wave absolute momentum flux and of its vertical gradient during recent stratospheric warmings. Atmospheric Chemistry and Physics, 2016, 16, 9983-10019.	1.9	59

#	Article	IF	CITATIONS
37	Long-range transport pathways of tropospheric source gases originating in Asia into the northern lower stratosphere during the Asian monsoon season 2012. Atmospheric Chemistry and Physics, 2016, 16, 15301-15325.	1.9	57
38	Lagrangian simulations of the transport of young air masses to the top of the Asian monsoon anticyclone and into the tropical pipe. Atmospheric Chemistry and Physics, 2019, 19, 6007-6034.	1.9	57
39	Gravity waves resolved in ECMWF and measured by SABER. Geophysical Research Letters, 2009, 36, .	1.5	52
40	Tidal signatures in temperature data from CRISTA 1 mission. Journal of Geophysical Research, 1999, 104, 16391-16403.	3.3	51
41	CRISTA observations of cirrus clouds around the tropopause. Journal of Geophysical Research, 2002, 107, CRI 2-1-CRI 2-18.	3.3	51
42	Differences in gravity wave drag between realistic oblique and assumed vertical propagation. Journal of Geophysical Research D: Atmospheres, 2014, 119, 10,081.	1.2	51
43	First tomographic observations of gravity waves by the infrared limb imager GLORIA. Atmospheric Chemistry and Physics, 2017, 17, 14937-14953.	1.9	51
44	Seasonal cycles and variability of O <sub>3</sub> and H <sub>2</sub> O in the UT/LMS during SPURT. Atmospheric Chemistry and Physics, 2006, 6, 109-125.	1.9	48
45	Variability of stratospheric mean age of air and of the local effects of residual circulation and eddy mixing. Journal of Geophysical Research D: Atmospheres, 2015, 120, 716-733.	1.2	48
46	Response of stratospheric water vapor and ozone to the unusual timing of El Niño and the QBO disruption in 2015–2016. Atmospheric Chemistry and Physics, 2018, 18, 13055-13073.	1.9	48
47	Instrument concept and preliminary performance analysis of GLORIA. Advances in Space Research, 2006, 37, 2287-2291.	1.2	47
48	Measurements of trace gases by the cryogenic infrared spectrometers and telescopes for the atmosphere (CRISTA) experiment. Advances in Space Research, 1997, 19, 563-566.	1.2	46
49	Satellite observations of middle atmosphere–thermosphere vertical coupling by gravity waves. Annales Geophysicae, 2018, 36, 425-444.	0.6	45
50	Driving of the SAO by gravity waves as observed from satellite. Annales Geophysicae, 2015, 33, 483-504.	0.6	43
51	CRISTA-2 observations of the South Polar Vortex in winter 1997: A new dataset for polar process studies. Geophysical Research Letters, 2001, 28, 3159-3162.	1.5	42
52	Comparison of satellite ozone observations in coincident air masses in early November 1994. Journal of Geophysical Research, 2001, 106, 9923-9943.	3.3	40
53	FORUM: Unique Far-Infrared Satellite Observations to Better Understand How Earth Radiates Energy to Space. Bulletin of the American Meteorological Society, 2020, 101, E2030-E2046.	1.7	40
54	Energy released by recombination of atomic oxygen and related species at mesopause heights. Journal of Geophysical Research, 1994, 99, 14585.	3.3	39

#	Article	IF	CITATIONS
55	Stratospheric transport by planetary wave mixing as observed during CRISTA-2. Journal of Geophysical Research, 2002, 107, CRI 7-1-CRI 7-13.	3.3	39
56	Three-dimensional simulation of stratospheric trace gas distributions measured by CRISTA. Journal of Geophysical Research, 1999, 104, 16419-16435.	3.3	38
57	Ozone loss driven by nitrogen oxides and triggered by stratospheric warmings can outweigh the effect of halogens. Journal of Geophysical Research, 2007, 112, .	3.3	38
58	Retrieval of three-dimensional small-scale structures in upper-tropospheric/lower-stratospheric composition as measured by GLORIA. Atmospheric Measurement Techniques, 2015, 8, 81-95.	1.2	38
59	A climatology of polar stratospheric cloud composition between 2002 and 2012 based on MIPAS/Envisat observations. Atmospheric Chemistry and Physics, 2018, 18, 5089-5113.	1.9	38
60	Fast cloud parameter retrievals of MIPAS/Envisat. Atmospheric Chemistry and Physics, 2012, 12, 7135-7164.	1.9	37
61	Satellite observations of cirrus clouds in the Northern Hemisphere lowermost stratosphere. Atmospheric Chemistry and Physics, 2015, 15, 927-950.	1.9	37
62	Global distribution of atomic oxygen in the mesopause region as derived from SCIAMACHY O( <sup>1</sup> S) green line measurements. Geophysical Research Letters, 2014, 41, 6274-6280.	1.5	36
63	A comprehensive observational filter for satellite infrared limb sounding of gravity waves. Atmospheric Measurement Techniques, 2015, 8, 1491-1517.	1.2	36
64	Observations of PAN and its confinement in the Asian summer monsoon anticyclone in high spatial resolution. Atmospheric Chemistry and Physics, 2016, 16, 8389-8403.	1.9	36
65	SOUTHTRAC-GW: An Airborne Field Campaign to Explore Gravity Wave Dynamics at the World's Strongest Hotspot. Bulletin of the American Meteorological Society, 2021, 102, E871-E893.	1.7	36
66	Dehydration and low ozone in the tropopause layer over the Asian monsoon caused by tropical cyclones: Lagrangian transport calculations using ERA-Interim and ERA5 reanalysis data. Atmospheric Chemistry and Physics, 2020, 20, 4133-4152.	1.9	35
67	Modeling the diurnal tide for the Cryogenic Infrared Spectrometers and Telescopes for the Atmosphere (CRISTA) 1 time period. Journal of Geophysical Research, 2000, 105, 24917-24929.	3.3	34
68	Hemispheric asymmetries and seasonality of mean age of air in the lower stratosphere: Deep versus shallow branch of the Brewerâ€Đobson circulation. Journal of Geophysical Research D: Atmospheres, 2015, 120, 2053-2066.	1.2	34
69	Impact of the Asian monsoon on the extratropical lower stratosphere: trace gas observations during TACTS over Europe 2012. Atmospheric Chemistry and Physics, 2016, 16, 10573-10589.	1.9	34
70	Shift of subtropical transport barriers explains observed hemispheric asymmetry of decadal trends of age of air. Atmospheric Chemistry and Physics, 2017, 17, 11177-11192.	1.9	34
71	Model simulations of stratospheric ozone loss caused by enhanced mesospheric NO <sub>x</sub> during Arctic Winter 2003/2004. Atmospheric Chemistry and Physics, 2008, 8, 5279-5293.	1.9	33
72	Tuning of a convective gravity wave source scheme based on HIRDLS observations. Atmospheric Chemistry and Physics, 2016, 16, 7335-7356.	1.9	33

#	Article	IF	CITATIONS
73	A highly miniaturized satellite payload based on a spatial heterodyne spectrometer for atmospheric temperature measurements in the mesosphere and lower thermosphere. Atmospheric Measurement Techniques, 2018, 11, 3861-3870.	1.2	33
74	Tomographic retrieval approach for mesoscale gravity wave observations by the PREMIER Infrared Limb-Sounder. Atmospheric Measurement Techniques, 2010, 3, 339-354.	1.2	33
75	High resolution limb observations of clouds by the CRISTA-NF experiment during the SCOUT-O3 tropical aircraft campaign. Advances in Space Research, 2008, 42, 1765-1775.	1.2	32
76	CRISTA-NF measurements with unprecedented vertical resolution during the RECONCILE aircraft campaign. Atmospheric Measurement Techniques, 2012, 5, 1173-1191.	1.2	32
77	Impact of the 2009 major sudden stratospheric warming on the composition of the stratosphere. Atmospheric Chemistry and Physics, 2015, 15, 8695-8715.	1.9	32
78	The need for accurate longâ€ŧerm measurements of water vapor in the upper troposphere and lower stratosphere with global coverage. Earth's Future, 2016, 4, 25-32.	2.4	32
79	Filamentary structure in chemical tracer distributions near the subtropical jet following a wave breaking event. Atmospheric Chemistry and Physics, 2013, 13, 10517-10534.	1.9	30
80	Volcanic ash detection with infrared limb sounding: MIPAS observations and radiative transfer simulations. Atmospheric Measurement Techniques, 2014, 7, 1487-1507.	1.2	30
81	Level 2 processing for the imaging Fourier transform spectrometer GLORIA: derivation and validation of temperature and trace gas volume mixing ratios from calibrated dynamics mode spectra. Atmospheric Measurement Techniques, 2015, 8, 2473-2489.	1.2	30
82	High tropospheric ozone in Lhasa within the Asian summer monsoon anticyclone in 2013: influence of convective transport and stratospheric intrusions. Atmospheric Chemistry and Physics, 2018, 18, 17979-17994.	1.9	30
83	Spectral wave analysis at the mesopause from SCIAMACHY airglow data compared to SABER temperature spectra. Annales Geophysicae, 2009, 27, 407-416.	0.6	30
84	Lidar observation and model simulation of a volcanic-ash-induced cirrus cloud during the Eyjafjallajökull eruption. Atmospheric Chemistry and Physics, 2012, 12, 10281-10294.	1.9	29
85	Sensitivity of Arctic ozone loss to stratospheric H <sub>2</sub> 0. Geophysical Research Letters, 2008, 35, .	1.5	28
86	CRISTA-NF measurements of water vapor during the SCOUT-O3 Tropical Aircraft Campaign. Advances in Space Research, 2009, 43, 74-81.	1.2	28
87	Impact of a possible future global hydrogen economy on Arctic stratospheric ozone loss. Energy and Environmental Science, 2012, 5, 6445.	15.6	28
88	Extending water vapor trend observations over Boulder into the tropopause region: Trend uncertainties and resulting radiative forcing. Journal of Geophysical Research D: Atmospheres, 2013, 118, 11269-11284.	1.2	28
89	Significant Contributions of Volcanic Aerosols to Decadal Changes in the Stratospheric Circulation. Geophysical Research Letters, 2017, 44, 10,780.	1.5	28
90	Zonally resolved impact of ENSO on the stratospheric circulation and water vapor entry values. Journal of Geophysical Research D: Atmospheres, 2016, 121, 11,486.	1.2	27

#	Article	IF	CITATIONS
91	How robust are stratospheric age of air trends from different reanalyses?. Atmospheric Chemistry and Physics, 2019, 19, 6085-6105.	1.9	27
92	Structural changes in the shallow and transition branch of the Brewer–Dobson circulation induced by El Niño. Atmospheric Chemistry and Physics, 2019, 19, 425-446.	1.9	27
93	Water vapor at the tropopause during the CRISTA 2 mission. Journal of Geophysical Research, 2002, 107, CRI 4-1-CRI 4-18.	3.3	26
94	Vibrationally excited ozone in the middle atmosphere. Journal of Atmospheric and Solar-Terrestrial Physics, 2006, 68, 202-212.	0.6	26
95	Impact of stratospheric major warmings and the quasiâ€biennial oscillation on the variability of stratospheric water vapor. Geophysical Research Letters, 2015, 42, 4599-4607.	1.5	25
96	Intercomparison of satellite and aircraft observations of ozone, CFC-11, and NOyusing trajectory mapping. Journal of Geophysical Research, 1999, 104, 16379-16390.	3.3	24
97	Retrieval of CFC-11 and CFC-12 from Envisat MIPAS observations by means of rapid radiative transfer calculations. Advances in Space Research, 2005, 36, 915-921.	1.2	24
98	A stratospheric intrusion at the subtropical jet over the Mediterranean Sea: air-borne remote sensing observations and model results. Atmospheric Chemistry and Physics, 2012, 12, 8423-8438.	1.9	24
99	Infrared limb emission measurements of aerosol in the troposphere and stratosphere. Atmospheric Measurement Techniques, 2016, 9, 4399-4423.	1.2	24
100	The stratospheric Brewer–Dobson circulation inferred from age of air in the ERA5 reanalysis. Atmospheric Chemistry and Physics, 2021, 21, 8393-8412.	1.9	24
101	Cryogenic infrared spectrometers and telescopes for the atmosphere: new frontiers. , 2004, , .		23
102	Scattering in infrared radiative transfer: A comparison between the spectrally averaging model JURASSIC and the line-by-line model KOPRA. Journal of Quantitative Spectroscopy and Radiative Transfer, 2013, 127, 102-118.	1.1	23
103	Multitimescale variations in modeled stratospheric water vapor derived from three modern reanalysis products. Atmospheric Chemistry and Physics, 2019, 19, 6509-6534.	1.9	23
104	Evidence of small-scale quasi-isentropic mixing in ridges of extratropical baroclinic waves. Atmospheric Chemistry and Physics, 2019, 19, 12607-12630.	1.9	23
105	CRISTA-NF measurements during the AMMA-SCOUT-O3 aircraft campaign. Atmospheric Measurement Techniques, 2010, 3, 1437-1455.	1.2	22
106	What causes the irregular cycle of the atmospheric tape recorder signal in HCN?. Geophysical Research Letters, 2010, 37, .	1.5	22
107	Water vapor increase in the lower stratosphere of the Northern Hemisphere due to the Asian monsoon anticyclone observed during the TACTS/ESMVal campaigns. Atmospheric Chemistry and Physics, 2018, 18, 2973-2983.	1.9	22
108	The semiannual oscillation (SAO) in the tropical middle atmosphere and its gravity wave driving in reanalyses and satellite observations. Atmospheric Chemistry and Physics, 2021, 21, 13763-13795.	1.9	22

#	Article	IF	CITATIONS
109	MIPAS observation of polar stratospheric clouds in the Arctic 2002/2003 and Antarctic 2003 winters. Advances in Space Research, 2005, 36, 868-878.	1.2	21
110	lce particle sampling from aircraft – influence of the probing position on the ice water content. Atmospheric Measurement Techniques, 2018, 11, 4015-4031.	1.2	21
111	A multi-wavelength classification method for polar stratospheric cloud types using infrared limb spectra. Atmospheric Measurement Techniques, 2016, 9, 3619-3639.	1.2	21
112	Cryogenic Infrared Spectrometers and Telescopes for the Atmosphere (CRISTA) observations of tracer transport by inertially unstable circulations. Journal of Geophysical Research, 1999, 104, 19171-19182.	3.3	20
113	How homogeneous and isotropic is stratospheric mixing? Comparison of CRISTA-1 observations with transport studies based on the Chemical Lagrangian Model of the Stratosphere (CLaMS). Quarterly Journal of the Royal Meteorological Society, 2005, 131, 565-579.	1.0	20
114	Chemical heating rates derived from SCIAMACHY vibrationally excited OH limb emission spectra. Advances in Space Research, 2008, 41, 1914-1920.	1.2	20
115	Intercomparison between Lagrangian and Eulerian simulations of the development of mid-latitude streamers as observed by CRISTA. Atmospheric Chemistry and Physics, 2005, 5, 85-95.	1.9	19
116	Stratospheric loss and atmospheric lifetimes of CFC-11 and CFC-12 derived from satellite observations. Atmospheric Chemistry and Physics, 2013, 13, 4253-4263.	1.9	19
117	The efficiency of transport into the stratosphere via the Asian and North American summer monsoon circulations. Atmospheric Chemistry and Physics, 2019, 19, 15629-15649.	1.9	19
118	Tomographic reconstruction of atmospheric gravity wave parameters from airglow observations. Atmospheric Measurement Techniques, 2017, 10, 4601-4612.	1.2	18
119	Chemical ozone loss in a chemistry-climate model from 1960 to 1999. Geophysical Research Letters, 2006, 33, .	1.5	17
120	Nighttime atomic oxygen in the mesopause region retrieved from SCIAMACHY O( <sup>1</sup> S) green line measurements and its response to solar cycle variation. Journal of Geophysical Research: Space Physics, 2015, 120, 9057-9073.	0.8	17
121	Sensitivities of modelled water vapour in the lower stratosphere: temperature uncertainty, effects of horizontal transport and small-scale mixing. Atmospheric Chemistry and Physics, 2018, 18, 8505-8527.	1.9	17
122	Upper tropospheric water vapour and its interaction with cirrus clouds as seen from IAGOS long-term routine in situ observations. Faraday Discussions, 2017, 200, 229-249.	1.6	16
123	Global analysis for periodic variations in gravity wave squared amplitudes and momentum fluxes in the middle atmosphere. Annales Geophysicae, 2019, 37, 487-506.	0.6	16
124	Comparison of simulated and observed convective gravity waves. Journal of Geophysical Research D: Atmospheres, 2016, 121, 13,474.	1.2	15
125	El Niño Southern Oscillation influence on the Asian summer monsoon anticyclone. Atmospheric Chemistry and Physics, 2018, 18, 8079-8096.	1.9	15
126	Removing spurious inertial instability signals from gravity wave temperature perturbations using spectral filtering methods. Atmospheric Measurement Techniques, 2020, 13, 4927-4945.	1.2	15

#	Article	IF	CITATIONS
127	Propagation paths and source distributions of resolved gravity waves in ECMWF-IFS analysis fields around the southern polar night jet. Atmospheric Chemistry and Physics, 2021, 21, 18641-18668.	1.9	15
128	Planetary wave two signatures in CRISTA 2 ozone and temperature data. Geophysical Monograph Series, 2000, , 319-325.	0.1	14
129	Sea surface temperature as a proxy for convective gravity wave excitation: a study based on global gravity wave observations in the middle atmosphere. Annales Geophysicae, 2014, 32, 1373-1394.	0.6	14
130	Limited angle tomography of mesoscale gravity waves by the infrared limb-sounder GLORIA. Atmospheric Measurement Techniques, 2018, 11, 4327-4344.	1.2	13
131	Lagrangian simulation of ice particles and resulting dehydration in the polar winter stratosphere. Atmospheric Chemistry and Physics, 2019, 19, 543-563.	1.9	13
132	Stratospheric Moistening After 2000. Geophysical Research Letters, 2022, 49, .	1.5	13
133	Observations of filamentary structures near the vortex edge in the Arctic winter lower stratosphere. Atmospheric Chemistry and Physics, 2013, 13, 10859-10871.	1.9	12
134	Retrieval of water vapor in the tropopause region from CRISTA measurements. Advances in Space Research, 2001, 27, 1635-1640.	1.2	11
135	Long-term changes of hydrogen-containing species in the stratosphere. Journal of Atmospheric and Solar-Terrestrial Physics, 2006, 68, 1973-1979.	0.6	11
136	Radiance calibration of CRISTA-NF. Advances in Space Research, 2009, 43, 1910-1917.	1.2	11
137	Validation of first chemistry mode retrieval results from the new limb-imaging FTS GLORIA with correlative MIPAS-STR observations. Atmospheric Measurement Techniques, 2015, 8, 2509-2520.	1.2	11
138	Superposition of gravity waves with different propagation characteristics observed by airborne and space-borne infrared sounders. Atmospheric Chemistry and Physics, 2020, 20, 11469-11490.	1.9	11
139	A detection method for cirrus clouds using CRISTA 1 and 2 measurements. Advances in Space Research, 2001, 27, 1629-1634.	1.2	10
140	NOypartitioning and aerosol influences in the stratosphere. Journal of Geophysical Research, 2002, 107, CRI 11-1-CRI 11-14.	3.3	10
141	CFC11 measurements by CRISTA. Advances in Space Research, 1997, 19, 575-578.	1.2	9
142	Assessment of the interannual variability and influence of the QBO and upwelling on tracer–tracer distributions of N <sub>2</sub> O and O <sub>3</sub> in the tropical lower stratosphere. Atmospheric Chemistry and Physics, 2013, 13, 3619-3641.	1.9	9
143	Tropical Cyclones Reduce Ozone in the Tropopause Region Over the Western Pacific: An Analysis of 18AYears Ozonesonde Profiles. Earth's Future, 2021, 9, e2020EF001635.	2.4	9
144	Orographically induced spontaneous imbalance within the jet causing a large-scale gravity wave event. Atmospheric Chemistry and Physics, 2021, 21, 10393-10412.	1.9	9

#	Article	IF	CITATIONS
145	3-D tomographic observations of Rossby wave breaking over the North Atlantic during the WISE aircraft campaign in 2017. Atmospheric Chemistry and Physics, 2021, 21, 10249-10272.	1.9	9
146	Evidence of H2O nonlocal thermodynamic equilibrium emission near 6.4 μm as measured by cryogenic infrared spectrometers and telescopes for the atmosphere (CRISTA 1). Journal of Geophysical Research, 2000, 105, 29003-29021.	3.3	8
147	Backtrajectory reconstruction of water vapour and ozone in-situ observations in the TTL. Meteorologische Zeitschrift, 2012, 21, 239-244.	0.5	8
148	Tropospheric mixing and parametrization of unresolved convective updrafts as implemented in the Chemical Lagrangian Model of the Stratosphere (CLaMS v2.0). Geoscientific Model Development, 2019, 12, 2441-2462.	1.3	8
149	Thermally stable monolithic Doppler asymmetric spatial heterodyne interferometer: optical design and laboratory performance. Optics Express, 2020, 28, 19887.	1.7	8
150	Modeling of nitrogen species measured by CRISTA. Geophysical Research Letters, 2000, 27, 2221-2224.	1.5	7
151	Quantitative transport studies based on trace gas assimilation. Advances in Space Research, 2004, 33, 1068-1072.	1.2	7
152	On the assembly and calibration of a spatial heterodyne interferometer for limb sounding of the middle atmosphere. CEAS Space Journal, 2019, 11, 525-531.	1.1	7
153	Analysis and correction of distortions in a spatial heterodyne spectrometer system. Applied Optics, 2019, 58, 2190.	0.9	7
154	Effective wind and temperature retrieval from Doppler asymmetric spatial heterodyne spectrometer interferograms. Applied Optics, 2018, 57, 8829.	0.9	7
155	Three-dimensional tomographic reconstruction of atmospheric gravity waves in the mesosphere and lower thermosphere (MLT). Atmospheric Measurement Techniques, 2018, 11, 3161-3175.	1.2	6
156	3-D tomographic limb sounder retrieval techniques: irregular grids and Laplacian regularisation. Atmospheric Measurement Techniques, 2019, 12, 853-872.	1.2	6
157	Aerosol and cloud top height information of Envisat MIPAS measurements. Atmospheric Measurement Techniques, 2020, 13, 1243-1271.	1.2	6
158	The Response of Atomic Hydrogen to Solar Radiation Changes. Springer Atmospheric Sciences, 2013, , 171-188.	0.4	6
159	Investigation on a SmallSat CMOS image sensor for atmospheric temperature measurement. , 2019, , .		6
160	A case study on the impact of severe convective storms on the water vapor mixing ratio in the lower mid-latitude stratosphere observed in 2019 over Europe. Atmospheric Chemistry and Physics, 2022, 22, 1059-1079.	1.9	6
161	Regionally Resolved Diagnostic of Transport: A Simplified Forward Model for CO2. Journals of the Atmospheric Sciences, 2017, 74, 2689-2700.	0.6	5
162	Sampling bias adjustment for sparsely sampled satellite measurements applied to ACE-FTS carbonyl sulfide observations. Atmospheric Measurement Techniques, 2019, 12, 2129-2138.	1.2	5

#	Article	IF	CITATIONS
163	Global nighttime atomic oxygen abundances from GOMOS hydroxyl airglow measurements in the mesopause region. Atmospheric Chemistry and Physics, 2019, 19, 13891-13910.	1.9	5
164	Observation of cirrus clouds with GLORIA during the WISE campaign: detection methods and cirrus characterization. Atmospheric Measurement Techniques, 2021, 14, 3153-3168.	1.2	5
165	AtmoCube A1: airglow measurements in the mesosphere and lower thermosphere by spatial heterodyne interferometry. Journal of Applied Remote Sensing, 2019, 13, 1.	0.6	5
166	New calibration noise suppression techniques for the GLORIA limb imager. Atmospheric Measurement Techniques, 2015, 8, 3147-3161.	1.2	4
167	AÂcomparison of OH nightglow volume emission rates as measured by SCIAMACHY and SABER. Atmospheric Measurement Techniques, 2020, 13, 3033-3042.	1.2	4
168	Evidence for a zonally trapped diurnal tide in CRISTA temperatures. Advances in Space Research, 1997, 19, 579-582.	1.2	3
169	<title>Trace gas densities and dynamics at and above the tropopause as derived from CRISTA data</title> ., 2001, , .		3
170	A case study of trace gas transports near the tropopause. Advances in Space Research, 2004, 33, 1053-1057.	1.2	3
171	Retrieval of chlorofluorocarbon distributions from Envisat MIPAS measurements. , 2004, , .		3
172	Cirrus cloud shape detection by tomographic extinction retrievals from infrared limb emission sounder measurements. Atmospheric Measurement Techniques, 2020, 13, 7025-7045.	1.2	3
173	CRISTA ozone measurements/validation. Advances in Space Research, 1997, 19, 567-570.	1.2	2
174	Hemispheric asymmetry of chemical species and its effect on stratospheric ozone: Emphasis on halogen loading. Advances in Space Research, 1999, 24, 1631-1636.	1.2	2
175	Three-dimensional model simulations of CRISTA trace gas measurements. Advances in Space Research, 2000, 26, 971-974.	1.2	2
176	Tracer structures in the southern hemispheric middle stratosphere observed by CRISTA-1. Advances in Space Research, 2001, 27, 1623-1628.	1.2	2
177	A novel CubeSat payload for airglow measurements in the mesosphere and lower thermosphere. , 2018, , .		2
178	Recombination energy of atomic oxygen and related species at the mesopause. Advances in Space Research, 1994, 14, 177-180.	1.2	1
179	Measurements of stratospheric trace gases by a balloon-borne infrared spectrometer in France. Journal of Atmospheric and Solar-Terrestrial Physics, 1997, 59, 1747-1755.	0.6	1
180	Retrieval of Upper Tropospheric H2O from CRISTA-2 Observations. , 2004, , 149-153.		0

#	Article	IF	CITATIONS
181	Physical and Chemical Processes in the Upper Troposphere and Lower Stratosphere. The Reacting Atmosphere, 2014, , 19-25.	0.8	0
182	Towards high resolution infrared limb sounding of the upper troposphere / lower stratosphere (UTLS). , 2016, , .		0
183	Optical design and performance analysis of a CubeSat-sized limb sounder utilizing a spatial heterodyne spectrometer for the measurement of mesospheric temperature. , 2019, , .		0
184	Advances in the optical design of a spatial heterodyne interferometer deployed on a 6U-CubeSat for atmospheric research. , 2019, , .		0